Critical role of biomass burning aerosols in enhanced historical Indian Ocean warming

Yiqun Tian[1], Shineng Hu[1*], Clara Deser[2]

[1] *Division of Earth and Climate Sciences, Nicholas School of the Environment, Duke University, Durham, NC, USA*

[2] *Climate and Global Dynamics, National Center for Atmospheric Research, Boulder, CO, USA*

Revised, 2 April 2023

[*]**Corresponding author:** Shineng Hu (shineng.hu@duke.edu)

Division of Earth and Climate Sciences, Nicholas School of the Environment, Duke University

Abstract

The tropical Indian Ocean (TIO) has experienced enhanced surface warming relative to the tropical mean during the past century, but the underlying mechanisms remain unclear. Here we use single-forcing, large-ensemble coupled model simulations to demonstrate that changes of biomass burning (BMB) aerosols have played a critical role in this TIO relative warming. Although the BMB aerosol changes have little effect on global mean temperatures due to regional cancellation, they significantly influence the pattern of warming over the tropical oceans. In particular, the reduction of BMB aerosols over the Indian subcontinent induces a TIO warming, while the increase of BMB aerosols over South America and Africa causes a cooling of the tropical Pacific and Atlantic, respectively. The resultant TIO relative warming leads to prominent global climate changes, including a westward expanded Indo-Pacific warm pool, a fresher TIO due to enhanced rainfall, and an intensified North Atlantic jet stream affecting European hydroclimate.

The tropical oceans have warmed substantially over the past century, with pronounced regional structures (Fig. 1a). Relative to the tropical mean, sea surface temperature (SST) warming is enhanced in the TIO, western Pacific and eastern Atlantic, and suppressed in the central-eastern Pacific. The enhanced warming in the climatologically warm TIO has attracted much attention[1,2,3] as it has been suggested to cause a wide range of climate impacts via teleconnections, including a strengthened positive phase of North Atlantic Oscillation (NAO)[4], reduced Sahel rainfall[5], an enhanced Pacific Walker Circulation[6], the occurrence of a North Atlantic "warming hole"[7], and an intensified Atlantic Meridional Overturning Circulation[8].

The enhanced TIO warming relative to the tropical mean is a robust feature across different datasets (Supplementary Figs. 1&2) and is particularly evident after the 1950s (Supplementary Fig. 3). We find that the observed absolute TIO warming rate is subject to large data uncertainties, but is positively correlated with the tropical mean warming rate (Fig. 1c). One common feature to all the observational datasets investigated here is that the TIO warming is greater than the tropical-mean warming (Fig. 1d). Our analysis suggests that this TIO "relative

52   warming" trend remains a prominent feature regardless of the time period chosen for analysis

53   (Supplementary Fig. 2). The fact that the TIO has warmed faster than the tropical oceans on

54   average may imply an overall increase of TIO rainfall, therefore driving the TIO-induced global

55   teleconnections mentioned above, but whether TIO rainfall has indeed increased over the past

56   century remains under debate due partly to the lack of direct observations[9,10,11].

57

58   The physical mechanisms underlying the observed TIO relative warming remain unclear. Several

59   mechanisms have been proposed to explain the TIO absolute warming, including, for example,

60   the increase in greenhouse gas concentration[1,3] or changes in El Niño-Southern Oscillation

61   properties[2]. These mechanisms may not necessarily be applicable to TIO relative warming,

62   however. Given the critical role of relative SST changes in shaping the tropical rainfall pattern[12],

63   it is therefore important to address the following questions. Is the observed TIO relative warming

64   a response to external radiative forcing? Does internal climate variability play a role? If

65   externally forced, which radiative forcing agent (or agents) is responsible for the TIO relative

66   warming? These questions are difficult to tackle by relying solely on observations. To that end,

67   we analyze single-forcing, large-ensemble coupled model simulations together with available

68   observations, which has led us to identify a previously overlooked role for BMB aerosol forcing

69   in the historical TIO relative warming.

70

71   **Tropical SST response to historical BMB changes**

72   To explore the mechanisms of TIO warming, we use the set of initial-condition Large Ensembles

73   (LEs) conducted with Community Earth System Model version 1 (CESM1) (Methods). CESM1

74   is a widely used, fully coupled general circulation model (GCM) that participates in the Coupled

75   Model Intercomparison Project Phase 5 (CMIP5). The LE setting helps to separate the externally

76   forced climate response from internal climate variability[13]. In addition to the standard all-forcing

77   (ALL) historical LE simulations[14], we use the "all-but-one-forcing" LE simulations[15] to isolate

78   the impacts of greenhouse gases (GHG), anthropogenic aerosols (AAER), and biomass burning

79   aerosols (BMB). The historical portion of the simulations spans the period 1920-2005, and we

80   use the period 1925-2005 for analysis to remove some of the potential influence of ocean initial

81   condition memory. The main conclusions presented do not change if a different period (e.g.,

82   1930-2005) is used for analysis.

83

84   A recent study suggests that CMIP5 coupled climate models on average simulate largely uniform

85   surface warming over the tropical oceans and thus underestimate the historical TIO relative

86   warming rate compared to observations[16]. Although the ensemble-mean of the CESM1 ALL LE

87   underestimates the observed tropical-mean ocean warming rate (Fig. 1c), it captures the TIO

88   relative warming with good fidelity (Fig. 1b). This implies that the observed TIO relative

89   warming may be partly attributable to external forcing, according to CESM1. The observation-

90   CESM1 mismatches (e.g., the enhanced western Pacific warming) can result from multidecadal

91   internal variability, among other factors such as uncertainties in radiative forcing and model

92   mean-state biases. We note that the LE ensemble spread in simulated TIO SST variations, both

93   absolute and relative, encompasses the observed variations (Supplementary Fig. 3). Although the

94   LE ensemble seems to slightly underestimate the TIO absolute warming since 1925, its spread

95   well encompasses the observed TIO relative warming (Fig. 1d). These results indicate that the

96   model has a realistic depiction of the combined influences of natural variability and forced

97   response in TIO trends. Interestingly, we find that ensemble members that simulate stronger TIO

98   relative warming rates tend to show better agreement with the observed pattern of tropical

99   warming, quantified in terms of spatial correlation (Supplementary Fig. 4).

100

101   Given the complex set of radiative forcing changes over the past century, is there a primary

102   factor that drives the forced component of TIO relative warming in CESM1? To answer this

103   question, we investigate the impacts of individual forcing agents, including GHG, AAER, and

104   BMB using the "all-but-one-forcing" LEs. As expected, GHG and AAER are the two dominant

105   and partially offsetting drivers of tropical mean surface temperature trends during the past

106   century, while BMB plays a minor role (Fig. 2a). Next, we compute the standard deviation of all

107   the grid points in the ensemble-mean SST trend field and use it as a measure of spatial variance.

108   Interestingly, we find that BMB contributes significantly to the spatial variability of tropical SST

109   warming and is comparable to the contributions from GHG or AAER (Fig. 2b). As far as we

110   know, the impact of BMB on the spatial variability of tropical SST trends (i.e., the pattern) has

111   been overlooked in previous studies. More specifically, we find that BMB is the main driver of

112   the TIO relative warming in the historical period, as we elaborate below.

113

114 Fig. 3b-f shows the ensemble-mean 1925-2005 trends of tropical relative SST (i.e., absolute SST

115 minus tropical-mean SST; see Methods), associated with each specific radiative forcing. The

116 standard, all-forcing historical simulations exhibit a complex spatial structure with relative

117 warming located in the central equatorial Pacific, the southeastern tropical Pacific, the central-

118 eastern equatorial Atlantic, and almost the entire TIO (Fig. 3b). Our forcing decomposition

119 analysis suggests that although BMB contributes little to the absolute TIO SST trend, it acts as

120 the most important radiative forcing for the TIO relative warming (Fig. 3a). In contrast, GHG

121 and AAER are two leading factors for TIO absolute SST changes, consistent with previous

122 studies[3], but not for TIO relative SST. Within the TIO, both GHG and AAER induce a

123 hemispheric asymmetry in relative SST trends, but these patterns largely cancel out leaving only

124 weak net changes (Fig. 3d-f). In the Pacific and Atlantic, GHG leads to an equatorially enhanced

125 warming, a common feature identified in coupled GCMs[17,18]. The southeastern tropical Pacific

126 relative warming is mainly induced by AAER, which is not unexpected given the greater

127 anthropogenic aerosol loading in the Northern Hemisphere[19,20]. Below we will focus primarily

128 on the mechanisms and impacts of BMB-induced TIO relative warming.

129

130 **Mechanisms of BMB-induced TIO relative warming**

131 How do the historical BMB changes affect the tropical SST warming pattern? BMB alters the

132 radiative budget both at the top-of-atmosphere and the surface by absorbing and scattering solar

133 radiation directly and by influencing cloud properties via indirect and semi-direct effects[21]. The

134 net radiative forcing of BMB aerosols at the ocean surface is suggested to be negative, albeit

135 bearing large uncertainties, and it acts to cool the ocean. During 1925-2005, BMB aerosols have

136 significantly increased over Equatorial Asia, South America and Central Africa, but have greatly

137 decreased over the Indian subcontinent, primarily in the 1950s (Supplementary Fig. 5b)[22]. These

138 BMB aerosol changes which originate over land in turn affect the surrounding tropical oceans,

139 leading to an increase of aerosol optical depth (AOD) over the tropical Atlantic, the tropical

140 Pacific, and the far eastern TIO, and a decrease of AOD over most of the TIO (Supplementary

141 Fig. 5a). This spatial heterogeneity in BMB emissions gives rise to a pronounced structure in the

142 SST response, with relative warming over the TIO and relative cooling over the tropical Pacific

143 and Atlantic (Fig. 4b).

144

145 To uncover the atmospheric and oceanic adjustments to the BMB forcing, we conduct an ocean

146 mixed layer heat budget analysis following ref. 23 (Methods). Below we summarize the key

147 points of the methodology. The SST changes induced by external radiative forcing (here BMB)

148 can be decomposed as:

149
$$T^t \approx T^t_{SW} + T^t_{LW} + T^t_{SH} + T^t_{Ocn} + T^t_{LH,w} + T^t_{LH,RH} + T^t_{LH,\Delta T} \tag{1}$$

150 In Eq. (1), the simulated, ensemble-mean SST trend, denoted as T^t, is broken down

151 approximately into 7 components. It is worth noting that the sum of the 7 sub-terms (denoted as

152 T^t_{sum}) may not be expected to exactly match the model simulated T^t due to the assumptions

153 made through the derivation, e.g., a linearized bulk formula of latent heat flux (Methods). The

154 first 4 components represent the contributions from the long-term trends in shortwave radiative

155 flux T^t_{SW}, longwave radiative flux T^t_{LW}, sensible heat flux T^t_{SH}, and ocean dynamics T^t_{Ocn},

156 respectively. The last three components represent the contributions from the trends in surface

157 wind speed $T^t_{LH,w}$, relative humidity $T^t_{LH,RH}$, and air-sea temperature gradient $T^t_{LH,\Delta T}$, respectively,

158 via latent heat flux changes. The full derivations and the expression of each component are

159 shown in the Methods.

160

161 The sum of the 7 SST trend components (T^t_{sum}) agrees quite well with the tropical SST trend

162 response to BMB forcing (i.e., T^t) with a pattern correlation of 0.88, validating our methodology

163 (Fig. 4b, c). The biggest contributors to the BMB-induced TIO relative warming are T^t_{SW} and

164 $T^t_{LH,w}$, while T^t_{Ocn} contributes to the TIO absolute but not relative warming (Fig. 4a), as we will

165 further discuss in detail below.

166 • T^t_{SW}: To separate the BMB direct and indirect/semidirect effects, we split T^t_{SW} into the

167   clear-sky and cloud components (Fig. 4f; Supplementary Fig. 6). The BMB reduction

168   over the TIO increases the clear-sky shortwave radiation reaching the surface and induces

169   a local warming especially around the Indian subcontinent (*cf.* Supplementary Fig. 5),

170   while cloud changes contribute to the warming primarily near the equator. At the same

171   time, the BMB increase over the eastern Pacific and Atlantic cools these areas primarily

172   via clear-sky shortwave radiation, amplified by SW cloud feedbacks in the eastern

173   Pacific. Altogether, T^t_{SW} becomes the primary driver of the BMB-induced TIO relative

174   warming (Fig. 4a).

175   • $T_{LH,w}^t$: The anomalous easterly winds in the northern TIO and northwesterly winds in the

176   southern TIO oppose the background wind and cause decreases in surface wind speed

177   and thus latent heat flux, acting as a warming effect (Fig. 4h). In addition, a considerable

178   cooling due to the increase of wind speed is identified over the southeast subtropical

179   Pacific. In terms of TIO relative warming, $T_{LH,w}^t$ serves as the second largest contributor

180   (Fig. 4a).

181   • T_{Ocn}^t: The change in ocean heat transport induces a relatively complex warming/cooling

182   structure (Fig. 4d). The prominent warming in the western TIO is consistent with the

183   anomalous alongshore northerly winds that are expected to induce Ekman convergence

184   and downwelling near the coast. The equatorial Atlantic warming is associated with an

185   anomalous Ekman convergence due to the westerly wind anomalies, while the eastern

186   equatorial Pacific warming can potentially be explained by a weaker poleward heat

187   transport by the climatological Ekman divergence due to the cooling SSTs (Fig. 4b). As a

188   result, ocean heat transport changes only play a minor role in the TIO relative SST

189   changes (Fig. 4a).

190

191 The changes in air-sea temperature gradient generally act as a damping effect to the tropical SST

192 changes with a pattern correlation of -0.67 (Fig. 4i; cf. Fig. 4b), since a warmer SST tends to

193 enhance the air-sea temperature contrast favoring an enhanced latent heat release. Other terms in

194 the heat budget are relatively small in terms of TIO basin averaged SST changes, although they

195 can be non-negligible locally.

196

197 **Potential impacts of BMB-induced TIO relative warming**

198 The BMB-induced TIO relative warming can potentially have important impacts on regional and

199 global climate. First, the TIO relative warming leads to an increase of rainfall over most of the

200 TIO, while in contrast, the western Pacific cooling in response to BMB increases over Equatorial

201 Asia induces a local reduction in precipitation (Fig. 5a). Such a zonal dipole in rainfall anomalies

202 suggests a westward displacement of the Indo-western Pacific warm pool convective center,

203 although the magnitude of rainfall change is rather weak (~10% of the climatological rate over a

204 century). Consistent with the precipitation change dipole, the TIO becomes fresher while the

205 western Pacific becomes saltier (Fig. 5b). These changes are also seen in the all-forcing

206   experiments but with a greater amplitude (Supplementary Fig. 7), implying that BMB changes

207   may play a critical role in shaping the Indo-western Pacific warm pool rainfall change pattern in

208   the past century.

209

210   The BMB-induced local rainfall changes over the TIO and western Pacific can potentially lead to

211   far-reaching impacts via global teleconnections. For example, we find that the North Atlantic jet

212   stream is significantly enhanced and shifted northward by the BMB forcing (Fig. 5c), similar to

213   the jet strengthening seen in the all-forcing experiments (Supplementary Fig. 7). The enhanced

214   North Atlantic jet stream transports more water vapor towards northwestern Europe, enhancing

215   rainfall over the British Isles and Scandinavia and reducing it over southern Europe and the

216   Mediterranean (Fig. 5d; Supplementary Fig. 7). The BMB-induced changes in the North Atlantic

217   jet and the associated European rainfall pattern all suggest a shift towards the positive phase of

218   NAO, as observed in the past century[24]. The BMB-induced changes can explain about a half of

219   the NAO positive trend seen in the all-forcing experiments, while the other half comes mainly

220   from GHG-induced changes (Supplementary Fig. 8). Our results are broadly consistent with the

221   previous studies that argue a TIO warming can induce a positive NAO[4,7,8]. A more definitive

222   demonstration of the BMB-TIO-NAO linkage, particularly whether the BMB-induced Atlantic

223   jet strengthening is explained solely by the TIO relative warming or partially by other factors,

224   requires further investigation.

225

226   **Discussion**

227   Our findings with CESM1 "all-but-one-forcing" large ensembles imply that BMB may play a

228   more important role in historical climate change than previously thought. Although the BMB

229   impact on global mean temperature change may be secondary as compared with GHG or AAER,

230   it does significantly influence the pattern of warming. In fact, over 80% of global BMB

231   emissions have occurred in tropical regions[25], and we indeed find that the change in BMB is

232   critical in shaping the tropical SST warming pattern in the past century. In particular, BMB is the

233   dominant contributor to the forced component of TIO relative warming, at least compared to

234   GHG and AAER (Fig. 3; Supplementary Fig. 9). While observational data products also show

235   relative TIO warming, most of this warming occurs after 1960 with considerable uncertainty in

236   terms of magnitude (Supplementary Fig. 9). It is likely that internal variability also contributes

237   to the observed relative TIO SST record. The TIO relative warming induced by the BMB

238   aerosol changes leads to locally enhanced rainfall, which together with the BMB-induced

239   cooling of the western Pacific, potentially acts to shift the Indo-western Pacific warm pool

240   convective center westward. The BMB-induced tropical rainfall changes may in turn cause a

241   positive NAO phase and influence North Atlantic/European climate via atmospheric

242   teleconnections. To what extent the results presented in this study are model dependent needs to

243   be tested by other climate models conducting similar types of historical experiments isolating the

244   contribution of BMB aerosol changes, which is currently not a protocol for most models.

245

246   Our study points to an urgent need to accurately represent the chemical, microphysical, and

247   radiative properties of BMB aerosols in GCMs. In the past decades, enormous progress has been

248   made in BMB-related studies, including both field campaign observations[26-31] and the associated

249   modeling efforts[32,33,34]. Despite these tremendous advances, an accurate representation of the

250   influence of BMB aerosols in climate models remains challenging. For example, a recent study

251   suggests that BMB aerosols in most climate models are too absorbing, leading to a potential bias

252   in radiative forcing[35]. In contrast, another study argues that the absorbing nature of BMB

253   aerosols over the Southeast Atlantic is underestimated in most climate models[36]. Such

254   discrepancies have yet to be reconciled. Another recent study reports that a discontinuity in the

255   variability of prescribed BMB emissions between the satellite era and the prior period in some

256   climate models can rectify the modeled mean climate and generate a spurious warming[37]. As

257   continuous observational efforts remain necessary in the coming decades, developing proxies of

258   historical BMB aerosols[38] and modeling their physical and chemical properties, transport within

259   the atmosphere, interactions with clouds, and role in carbon cycle dynamics all need to be

260   refined. In that regard, modeling efforts like the Fire Modeling Intercomparison Project[34] will be

261   particularly helpful in interpreting and potentially reducing inter-model spread. Improving the

262   understanding and simulation of BMB aerosols thus requires the integrated efforts of worldwide

263   observational and laboratory communities, Earth science modeling communities, and more

264   importantly, the collaboration between those communities.

265 **Methods**

266

267 **Observational datasets**

268 We use four monthly observational SST datasets: 1. National Oceanic and Atmospheric

269 Administration Extended Reconstructed Sea Surface Temperature Version 5 (ERSSTv5) with

270 resolution 2°×2°[39]. 2. Hadley Centre Sea Ice and SST v.1.1 (HadISST 1.1) with resolution

271 1°×1°[40]. 3. Centennial In Situ Observation-Based Estimates of the Variability of SST and Marine

272 Meteorological Variables (COBE) with resolution 1°×1°[41]. 4. Kaplan Extended SST v2 with

273 resolution 5°×5°[42].

274

275 **CESM1 Large-Ensemble simulations**

276 We use four sets of simulations from the Community Earth System Model version 1 Large

277 Ensemble (CESM1-LE)[14] produced by the National Center for Atmospheric Research (NCAR).

278 The first set is the standard all-forcing (ALL) historical simulations which contains all historical

279 radiative forcings; it has 40 ensemble members. The other three sets are the CESM1-LE ''all-

280 but-one-forcing'' experiments[15], which are designed to isolate the influence of individual forcing

281 agents, including anthropogenic aerosols (AAER), greenhouse gases (GHG), and biomass

282 burning aerosols (BMB). They are identical to the all-forcing historical simulations (i.e., ALL)

283 except that one forcing agent is fixed at its 1920 level. More specifically, the XGHG (where "X"

284 refers to the fact that GHG is held fixed) set has 20 ensemble members with fixed GHG; the

285 XAAER set has 20 ensemble members with fixed AAER; the XBMB set has 15 ensemble

286 members with fixed BMB. Each ensemble member within each set starts from slightly different

287 atmospheric initial conditions on the order of 10^{-14}K. The influence of each individual forcing

288 agent can therefore be determined by subtracting ''all-but-one-forcing'' member-mean from

289 ALL member-mean, that is,

290 GHG = ALL ensemble mean – XGHG ensemble mean

291 AAER = ALL ensemble mean – XAAER ensemble mean

292 BMB = ALL ensemble mean – XBMB ensemble mean

293 The full time period for all the experiments under historical forcing is 1920-2005. To avoid the

294 potential influence of ocean initial conditions, we use the period 1925-2005.

295

Definitions of indices

For both observations and simulations, the tropics refers to the latitudinal band 20°S – 20°N, and the TIO refers to the region 20°S-20°N, 40°E-100°E. Relative SST is defined as the difference between local SST and tropical mean SST.

The NAO pattern and index used here are computed as the first EOF and PC of annual mean sea level pressure anomalies within the region of 20°N-80°N, 90°W-40°E, after concatenating all the members from ALL, XBMB, XAER and XGHG.

Ocean mixed layer heat budget analysis

To further understand the mechanisms of BMB-induced TIO warming, we conducted ocean mixed layer heat budget analysis following the methodology in ref. 23 and the references therein. The ocean surface mixed layer heat budget can be written as:

$$\rho C_p H \frac{\partial SST}{\partial t} = SW + LW + SH + LH + Ocn. \tag{1}$$

The left-hand side represents mixed layer heat storage, where ρ is density of sea water, C_p is specific heat of sea water, H is depth of ocean mixed layer and SST is temperature of ocean mixed layer. On the right-hand side, SW is surface net shortwave radiative flux, LW is surface net longwave flux, SH is surface sensible heat flux, LH is surface latent heat flux and Ocn is the heat flux due to ocean dynamics. We then do the linear regression to Eq. (1). Since the trend of ocean mixed layer heat storage can be treated as negligible[12,43], the left-hand side becomes zero and we have:

$$0 = SW^t + LW^t + SH^t + LH^t + Ocn^t \tag{2}$$

We define downward as positive and the superscript t represents BMB induced ensemble mean trend during 1925-2005. Latent heat flux term is directly related to SST and can be written as:

$$LH = -\rho_{air} L_v C_E W [q^*(SST) - q_{air}] \tag{3}$$

q_{air} in Eq. (3) is specific humidity of air above sea surface. It can be expressed as:

$$q_{air} = RH q^*(SST - \Delta T) \tag{4}$$

Where RH is relative humidity at sea surface, ΔT is temperature gradient near sea surface and we define it as $(SST - T_{air})$. We further rewrite q_{air} by using Clausius-Clapeyron equation:

$$q_{air} = RH q^*(SST) e^{-\alpha \Delta T} \tag{5}$$

Where $\alpha \approx 0.06/K$. We plug Eq. (5) into Eq. (3) and get new latent heat flux expression:

327 $$LH = -\rho_{air} L_v C_E W q^*(SST)(1 - RHe^{-\alpha\Delta T})$$ (6)

328 Next, we use linear regression to get LH^t from Eq. (6):

329 $$LH^t = \frac{\partial LH}{\partial W} W^t + \frac{\partial LH}{\partial SST} SST^t + \frac{\partial LH}{\partial RH} RH^t + \frac{\partial LH}{\partial \Delta T} \Delta T^t$$

330 $$= \frac{\overline{LH}}{\overline{W}} W^t + \alpha\overline{LH} SST^t - \frac{\overline{LH}}{e^{\alpha\overline{\Delta T}} - \overline{RH}} RH^t + \frac{\alpha\overline{LH}\,\overline{RH}}{e^{\alpha\overline{\Delta T}} - \overline{RH}} \Delta T^t$$ (7)

331 where the overbar for $\overline{LH}, \overline{W}, \overline{\Delta T}, \overline{RH}$ is climatology computed using the period of 1925-1944.

332 Plugging in Eq. (7), we can then rewrite Eq. (2) as:

333 $$T^t \approx -\frac{SW^t + LW^t + SH^t + Ocn^t}{\alpha\overline{LH}} - \frac{W^t}{\alpha\overline{W}} - \frac{\overline{RH}\,\Delta T^t}{e^{\alpha\overline{\Delta T}} - \overline{RH}} + \frac{RH^t}{\alpha(e^{\alpha\overline{\Delta T}} - \overline{RH})}$$

334 $$= T_{SW}^t + T_{LW}^t + T_{SH}^t + T_{Ocn}^t + T_{LH,w}^t + T_{LH,RH}^t + T_{LH,\Delta T}^t$$ (8)

335 where SST^t is written as T^t for brevity. The last three terms are all related to latent heat flux

336 changes via the changes in surface wind speed $T_{LH,w}^t$, relative humidity $T_{LH,RH}^t$ and temperature

337 gradient $T_{LH,\Delta T}^t$, respectively. In summary, T^t can be split into seven sub-terms as follow:

338 $$T_{SW}^t = -\frac{SW^t}{\alpha\overline{LH}}$$ (9)

339 $$T_{LW}^t = -\frac{LW^t}{\alpha\overline{LH}}$$ (10)

340 $$T_{SH}^t = -\frac{SH^t}{\alpha\overline{LH}}$$ (11)

341 $$T_{Ocn}^t = -\frac{Ocn^t}{\alpha\overline{LH}}$$ (12)

342 $$T_{LH,w}^t = -\frac{W^t}{\alpha\overline{W}}$$ (13)

343 $$T_{LH,\Delta T}^t = -\frac{\overline{RH}\,\Delta T^t}{e^{\alpha\overline{\Delta T}} - \overline{RH}}$$ (14)

344 $$T_{LH,RH}^t = \frac{RH^t}{\alpha(e^{\alpha\overline{\Delta T}} - \overline{RH})}$$ (15)

345 It is worth noting that the sum of the seven sub-terms (T_{sum}^t) may not be expected to exactly

346 match the model simulated T^t due to the assumptions made through the derivation, e.g., a

347 linearized bulk formula of latent heat flux.

Code availability

All codes are available upon request.

Author contributions

Y. T. and S.H. conceived the original idea and wrote the first draft of the manuscript. Y.T.
performed the analysis. Y.T., S.H., and C.D. contributed to the interpretation of results and
edited the manuscript.

Competing interest

The authors declare that they have no competing interests.

Materials & Correspondence

Correspondence and requests for materials should be addressed to S. H.

References

1. Du, Y., & Xie, S. P. Role of atmospheric adjustments in the tropical Indian Ocean warming during the 20th century in climate models. *Geophys. Res. Lett.* https://doi.org/10.1029/2008GL033631 (2008).

2. Roxy, M. K., Ritika, K., Terray, P., & Masson, S. The curious case of Indian Ocean warming. *J. Clim.* **27,** 8501-8509 (2014).

3. Dong, L., & Zhou, T. The Indian Ocean sea surface temperature warming simulated by CMIP5 models during the twentieth century: Competing forcing roles of GHGs and anthropogenic aerosols. *J. Clim. 27,* 3348-3362 (2014).

4. Hoerling, M. P., Hurrell, J. W., & Xu, T. Tropical origins for recent North Atlantic climate change. *Science* **292**, 90-92 (2001).

5. Lu, J., & Delworth, T. L. Oceanic forcing of the late 20th century Sahel drought. *Geophys. Res. Lett.* https://doi.org/10.1029/2005GL023316 (2005).

6. Luo, J. J., Sasaki, W., & Masumoto, Y. Indian Ocean warming modulates Pacific climate change. *Proc. Natl Acad. Sci.* USA https://doi.org/10.1073/pnas.1210239109 (2012).

7. Hu, S., & Fedorov, A. V. Indian Ocean warming as a driver of the North Atlantic warming hole. *Nat. Commun.* **11,** 1-11 (2020).

8. Hu, S., & Fedorov, A. V. Indian Ocean warming can strengthen the Atlantic meridional overturning circulation. *Nat. Clim. Change* **9,** 747-751 (2019).

9. Hoerling, M. P., Hurrell, J. W., Xu, T., Bates, G. T., & Phillips, A. S. Twentieth century North Atlantic climate change. Part II: Understanding the effect of Indian Ocean warming. *Clim. Dyn.* **23,** 391-405 (2004).

10. Deser, C., Phillips, A. S., & Alexander, M. A. Twentieth century tropical sea surface temperature trends revisited. *Geophys. Res. Lett.* **37,** (2010).

11. Hu, S., & Seager, R. Revisiting the enhanced Indian Ocean warming since 1950: A major point of disagreement between observations and CMIP6 models, submitted.

12. Xie, S. P. et al. Global warming pattern formation: Sea surface temperature and rainfall. *J. Clim.* **23,** 966-986 (2010).

13. Deser, C. et al. Insights from Earth system model initial-condition large ensembles and future prospects. *Nat. Clim. Change 10,* 277-286 (2020).

406 14. Kay, J. E. et al. The Community Earth System Model (CESM) large ensemble project: A
407   community resource for studying climate change in the presence of internal climate
408   variability. *Bull. Am. Meteorol. Soc.* **96,** 1333-1349 (2015).
409 15. Deser, C. et al. Isolating the evolving contributions of anthropogenic aerosols and
410   greenhouse gases: a new CESM1 large ensemble community resource. *J. Clim.* **33,** 7835-
411   7858 (2020).
412 16. Zhang, L. et al. Indian Ocean warming trend reduces Pacific warming response to
413   anthropogenic greenhouse gases: An interbasin thermostat mechanism. *Geophys. Res.*
414   *Lett.* https://doi.org/10.1029/2019GL084088 (2019).
415 17. Liu, Z., Vavrus, S., He, F., Wen, N., & Zhong, Y. Rethinking tropical ocean response to
416   global warming: The enhanced equatorial warming. *J. Clim.* **18,** 4684-4700 (2005).
417 18. Heede, U. K., Fedorov, A. V., & Burls, N. J. Time scales and mechanisms for the tropical
418   Pacific response to global warming: A tug of war between the ocean thermostat and
419   weaker walker. *J. Clim.* **33,** 6101-6118 (2020).
420 19. Wang, H., Xie, S. P., & Liu, Q. Comparison of climate response to anthropogenic aerosol
421   versus greenhouse gas forcing: Distinct patterns. *J. Clim.* **29,** 5175-5188 (2016).
422 20. Shi, J. R., Kwon, Y. O., & Wijffels, S. E. Two Distinct Modes of Climate Responses to
423   the Anthropogenic Aerosol Forcing Changes. *J. Clim.* **35,** 3445-3457 (2022).
424 21. Liu, L. et al. Impact of biomass burning aerosols on radiation, clouds, and precipitation
425   over the Amazon: relative importance of aerosol–cloud and aerosol–radiation
426   interactions. *Atmos. Chem. Phys.* **20,** 13283-13301 (2020).
427 22. Lamarque, J. F. et al. Historical (1850–2000) gridded anthropogenic and biomass burning
428   emissions of reactive gases and aerosols: methodology and application. *Atmos. Chem.*
429   *Phys.* **10,** 7017-7039 (2010).
430 23. Zhang, X., Deser, C., & Sun, L. Is there a tropical response to recent observed Southern
431   Ocean cooling? *Geophys. Res. Lett.* https://doi.org/10.1029/2020GL091235 (2021).
432 24. Hurrell, J. W. Decadal trends in the North Atlantic Oscillation: Regional temperatures
433   and precipitation. *Science* **269,** 676-679 (1995).
434 25. Van Marle, M. J. et al. Historic global biomass burning emissions for CMIP6
435   (BB4CMIP) based on merging satellite observations with proxies and fire models (1750–
436   2015). *Geosci. Model Dev.* **10,** 3329-3357 (2017).

437   26. Kaufman, Y. J. et al. Smoke, clouds, and radiation-Brazil (SCAR-B) experiment. *J.*
438   *Geophys. Res. Atmos.* **103,** 31783-31808 (1998).

439   27. Delmas, R. A. et al. Experiment for Regional Sources and Sinks of Oxidants
440   (EXPRESSO): An overview, *J. Geophys. Res. Atmos.* **104,** 30609-30624 (1999).

441   28. Swap, R. J. et al. Africa burning: A thematic analysis of the Southern African Regional
442   Science Initiative (SAFARI 2000), *J. Geophys. Res. Atmos.* **108,** 8465 (2003).

443   29. Janicot, S. et al. Large-scale overview of the summer monsoon over West Africa during
444   the AMMA field experiment in 2006. *Annales Geophysicae* **26,** 2569-2595 (2008).

445   30. Abel, S. J. et al. Open cells exhibit weaker entrainment of free-tropospheric biomass
446   burning aerosol into the south-east Atlantic boundary layer. *Atmos. Chem. Phys.* **20,**
447   4059-4084 (202).

448   31. Redemann, J. et al. An overview of the ORACLES (ObseRvations of Aerosols above
449   CLouds and their intEractionS) project: aerosol–cloud–radiation interactions in the
450   southeast Atlantic basin. *Atmos. Chem. Phys.* **21,** 1507-1563 (2021).

451   32. Keil, A., & Haywood, J. M. Solar radiative forcing by biomass burning aerosol particles
452   during SAFARI 2000: A case study based on measured aerosol and cloud properties. *J.*
453   *Geophys. Res. Atmos.* **108,** 8467 (2003).

454   33. Haywood, J. M., Osborne, S. R., & Abel, S. J. The effect of overlying absorbing aerosol
455   layers on remote sensing retrievals of cloud effective radius and cloud optical depth. *Q. J.*
456   *R. Meteorol. Soc.* https://doi.org/10.1256/qj.03.100 (2004)

457   34. Rabin, S. S. et al. The Fire Modeling Intercomparison Project (FireMIP), phase 1:
458   experimental and analytical protocols with detailed model descriptions. *Geosci. Model*
459   *Dev.* **10,** 1175-1197 (2017).

460   35. Brown, H. et al. Biomass burning aerosols in most climate models are too absorbing. *Nat.*
461   *Commun.* **12,** 1-15 (2021).

462   36. Mallet, M. et al. Climate models generally underrepresent the warming by Central Africa
463   biomass-burning aerosols over the Southeast Atlantic. *Sci. Adv.* **7,** eabg9998 (2021).

464   37. Fasullo, J. T. et al. Spurious Late Historical-Era Warming in CESM2 Driven by
465   Prescribed Biomass Burning Emissions. *Geophys. Res. Lett.*
466   https://doi.org/10.1029/2021GL097420 (2022).

467   38. Marlon, J. R. et al. Reconstructions of biomass burning from sediment-charcoal records
468   to improve data–model comparisons. *Biogeosciences* **13,** 3225-3244 (2016).

469   39. Huang, B. et al. Extended reconstructed sea surface temperature, version 5 (ERSSTv5):
470   upgrades, validations, and intercomparisons. *J. Clim.* **30,** 8179-8205 (2017).

471   40. Rayner, N. A. A. et al. Global analyses of sea surface temperature, sea ice, and night
472   marine air temperature since the late nineteenth century. J. Geophys. Res. Atmos.
473   https://doi.org/10.1029/2002JD002670 (2003).

474   41. Ishii, M., Shouji, A., Sugimoto, S., & Matsumoto, T. Objective analyses of sea-surface
475   temperature and marine meteorological variables for the 20th century using ICOADS and
476   the Kobe collection. *Int. J. Climatol.* **25,** 865-879 (2005).

477   42. Kaplan, A. et al. Analyses of global sea surface temperature 1856–1991. *J. Geophys Res.*
478   *Oceans,* **103,** 18567-18589 (1998).

479   43. Cook, K. H., Vizy, E. K., & Sun, X. Multidecadal-scale adjustment of the ocean mixed
480   layer heat budget in the tropics: examining ocean reanalyses. *Clim. Dyn.* **50,** 1513-1532
481   (2018).
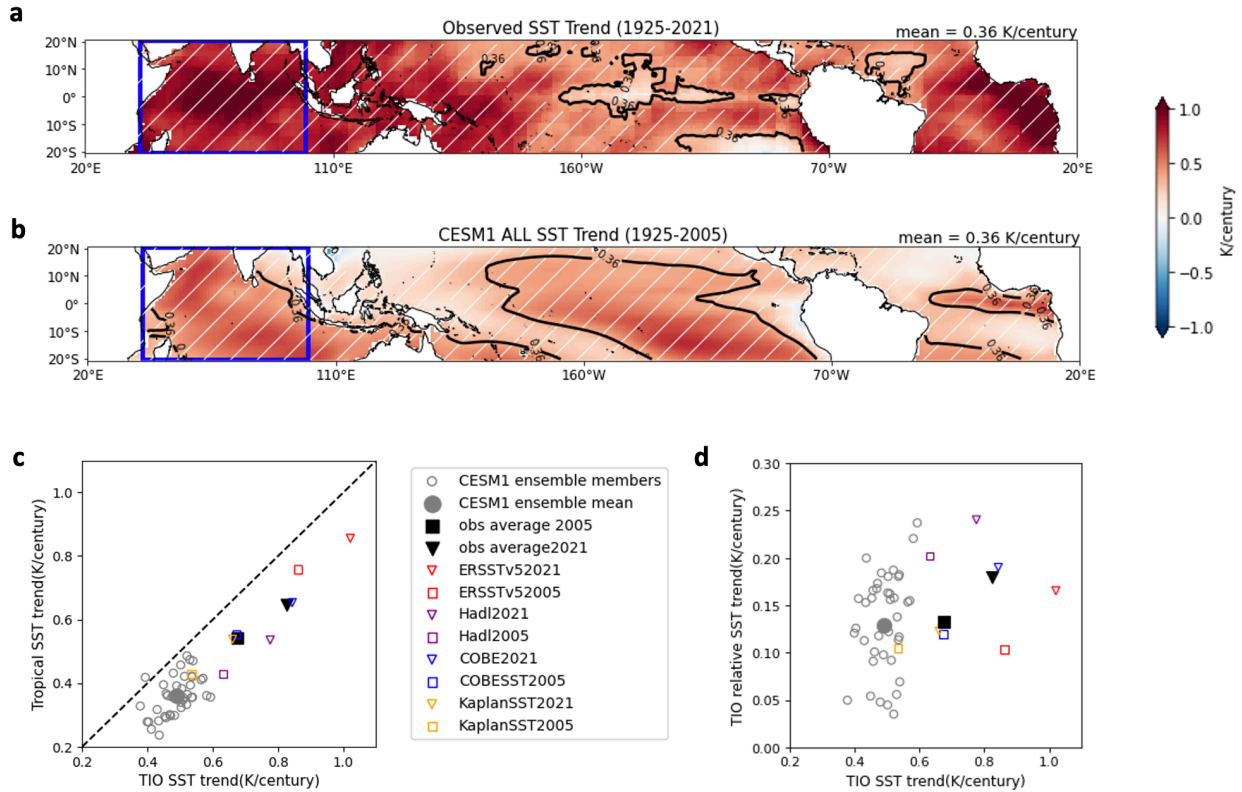
Fig. 1 | Observed and model simulated tropical SST trends since 1925. a, Observed tropical SST trends (K/century) during 1925-2021, averaged across four SST datasets (ERSSTv5, HadISST, COBE-SST, Kaplan SST). **b**, CESM1-LE ensemble-mean tropical SST trends (K/century) during 1925-2005 from the all-forcing experiments. In panels a and b, the black contour line represents the isopleth of the tropical-mean SST trend (values shown on the top-right corner). **c**, Simulated and observed TIO SST trends versus tropical-mean SST trends during 1925-2005. The observed trends during 1925-2021 are also shown for comparison. **d**, Similar to panel c but for TIO SST trends vs. TIO relative SST trends. Relative SST is defined as absolute SST minus tropical-mean SST. White hatches in **a** and **b** represent the regions that are 99% significant based on a t-test.

493
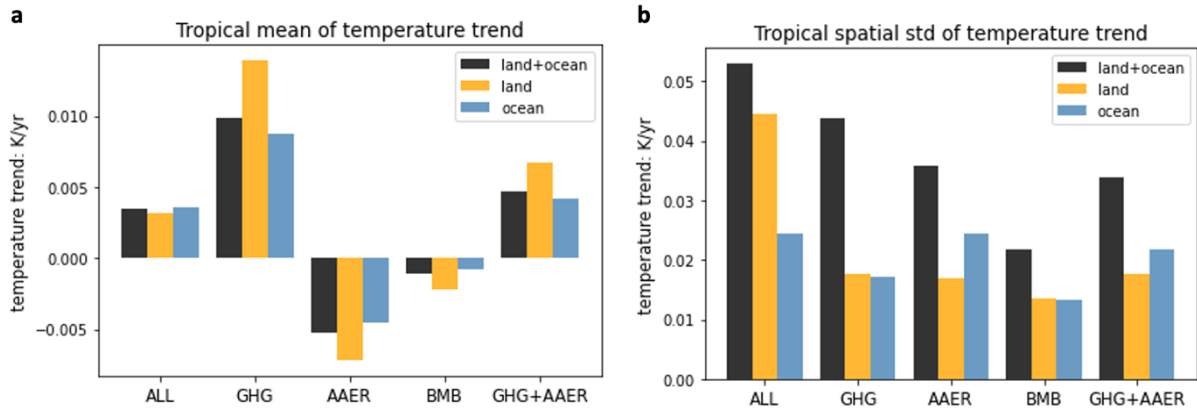
Fig. 2 | Attribution of tropical warming to individual radiative forcing agents in 1925-2005.

a, Ensemble-mean, tropical-mean surface temperature trends (K/year) attributed to each radiative forcing: all-forcing (ALL), greenhouse gas (GHG), anthropogenic aerosols (AAER), biomass burning aerosols (BMB), anthropogenic aerosols and greenhouse gas combined (AAER+GHG). For each forcing, calculations have been performed for land only, ocean only, and land-ocean combined. **b**, Similar to panel a but for spatial standard deviation of ensemble-mean SST trends in the tropics. For both panels, the tropics is defined as 20°S-20°N.
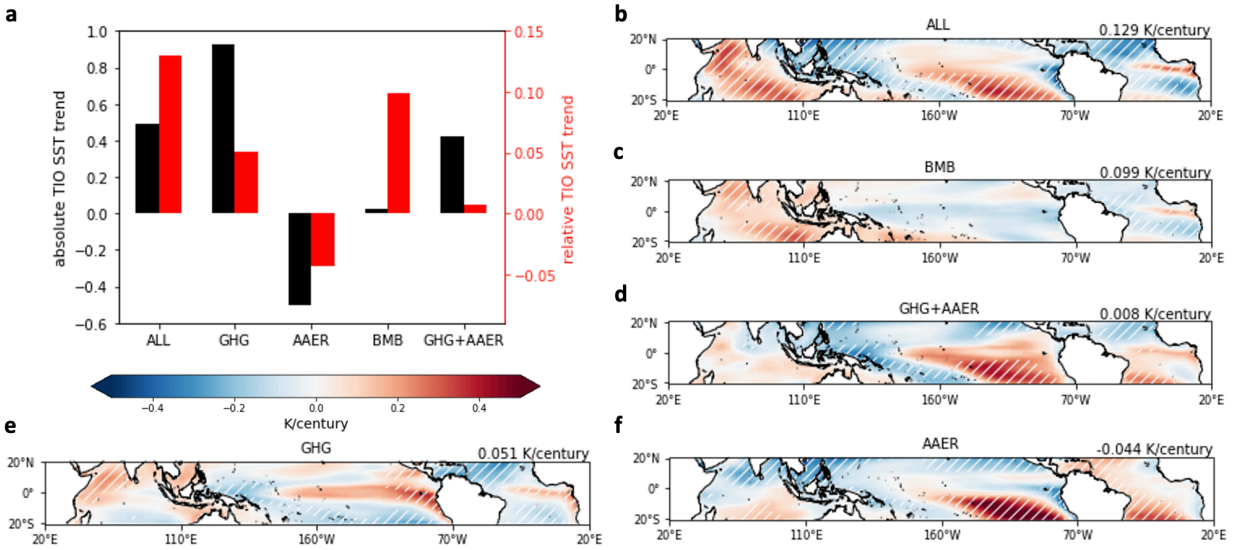
Fig. 3 | Critical role of BMB in the historical TIO relative warming. a, Absolute and relative TIO SST trends (K/century) during 1925-2005 attributed to individual radiative forcing agents, similar to Fig. 2. Note the two different vertical axes. **b-f**, Tropical relative SST trends (K/century) during 1925-2005 in all-forcing experiments and attributed to each radiative forcing. Relative SST is defined as absolute SST minus tropical-mean SST. The value on the top right corner represents the TIO-mean relative SST trend. White hatches in **b-f** represent the regions that are 99% significant based on a t-test.
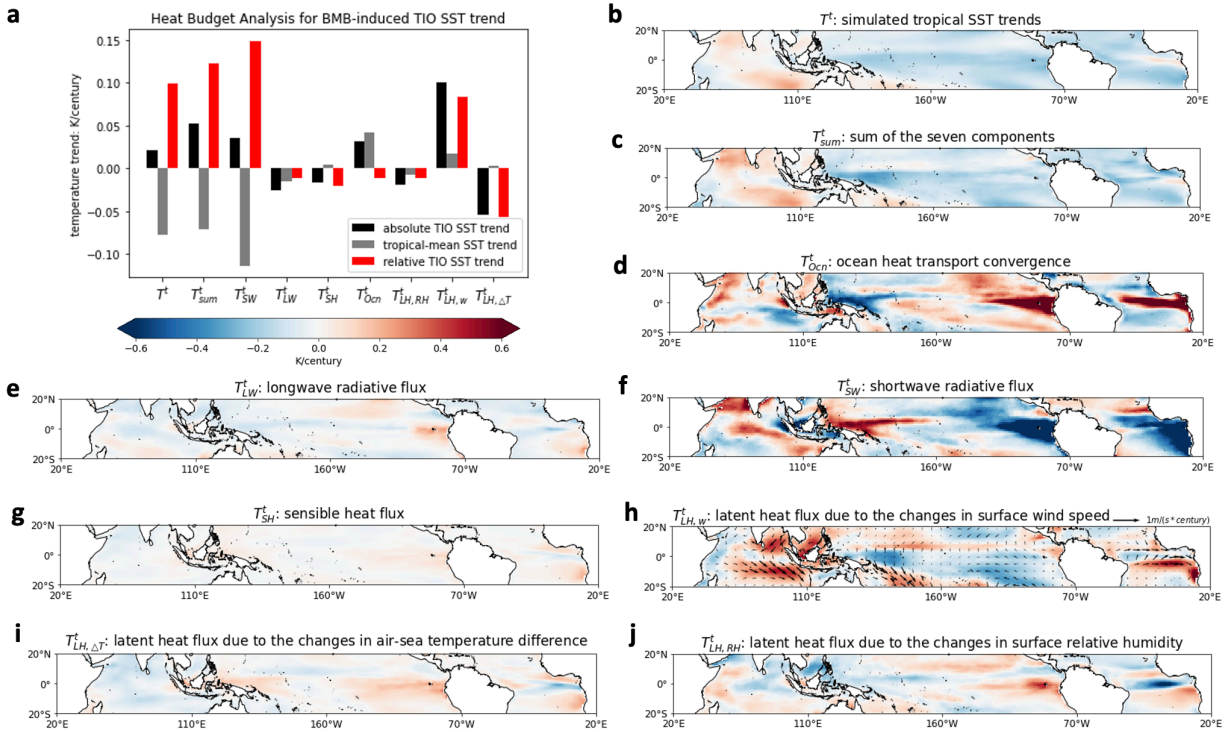
509

510 **Fig. 4 | Heat budget analysis for BMB-induced TIO warming. a**, TIO SST trends (K/century)

511 during 1925-2005 attributed to each component in the ocean-mixed layer heat budget (Methods).

512 The TIO absolute trends are further split into two components, tropical-mean SST trends and

513 TIO relative SST trends. **b**, Simulated tropical SST trends during 1925-2005 (K/century) induced

514 by BMB changes. **c-j**, BMB-induced tropical SST trends during 1925-2005 attributed to **c** sum of

515 the following seven components ($T_{sum}{}^{t}$), the changes in **d** ocean heat transport convergence

516 (T_{Ocn}^{t}), **e** longwave radiative flux (T_{LW}^{t}), **f** shortwave radiative flux (T_{SW}^{t}), **g** sensible heat flux

517 (T_{SH}^{t}), and latent heat flux due to the changes in **h** surface wind speed ($T_{LH,w}^{t}$), **i** air-sea

518 temperature difference ($T_{LH,\Delta T}^{t}$), and **j** surface relative humidity ($T_{LH,RH}^{t}$).

519
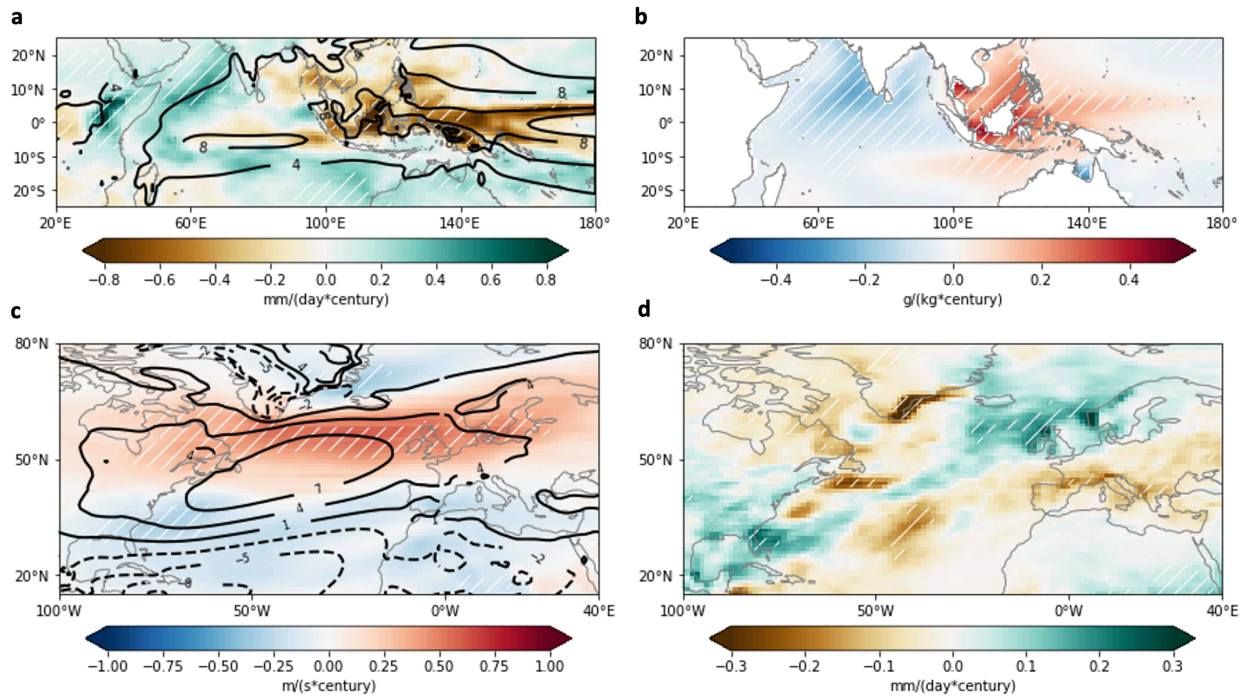
Fig. 5 | Potential climate impacts associated with BMB-induced TIO relative warming. a,
BMB-induced rainfall trends (colors; mm/d/century) overlaid by climatological rainfall
(contours; mm/d) and **b**, BMB-induced ocean salinity trends (g/kg/century) during 1925-2005. **c**,
BMB-induced 850 mb zonal wind trends (colors; m/s/century) overlaid by climatological 850 mb
zonal wind (contours; m/s) and **d**, BMB-induced rainfall trends (mm/d/century) during 1925-
2005. White hatches in **a-d** represent the regions that are 99% significant based on a t-test.